

## NUMERICAL SIMULATIONS OF BUBBLE DISPERSION OVER A HYDROFOIL

**S. J. ZHU<sup>1</sup>, A. Ooi<sup>1</sup>, H. M. BLACKBURN<sup>2</sup> and B. ANDERSON<sup>3</sup>**

<sup>1</sup> Department of Mechanical Engineering, Melbourne School of Engineering, The University of Melbourne, Victoria 3010, AUSTRALIA

<sup>2</sup> Department of Mechanical and Aerospace Engineering, Monash University, Victoria 3800, AUSTRALIA

<sup>3</sup> Maritime Platforms Division, Defence Science and Technology Organisation, Victoria 3207, AUSTRALIA

### ABSTRACT

The production and entrainment of bubbles in ship wakes is not completely understood despite the fact that it has many practical applications. For example, bubbles trapped in the large vortical structures in the ship wake can form clusters that are able to persist for large distances leaving a long trail of bubbles, which increases the ship's signature; an important consideration in the defence environment. This work presents numerical results on the effect of a hydrofoil on a population of bubbles as they pass over it, and the resulting distribution of bubbles downstream for a range of angles of attack and Reynolds numbers. Direct numerical simulation (DNS) is used with a Lagrangian particle tracking method, which is more suited for fundamental investigations of the bubbly flow. It is seen that the effect of the angle of attack on the downstream bubble distribution is small at low Reynolds number but the effect increases at higher Reynolds number. Our data also shows that the effect of angle of attack on downstream bubble distribution is more significant for  $\alpha = 20^\circ$  rather than for  $\alpha \leq 10^\circ$ .

### NOMENCLATURE

|                          |   |
|--------------------------|---|
| $c$                      | chord length of the hydrofoil   |
| $d_b$                    | bubble diameter   |
| $h$                      | time step   |
| $n_p$                    | number of Lagrange knot points along the side of each element                   |
| $p$                      | pressure  |
| $r_b$                    | bubble radius   |
| $t$                      | dimensional time  |
| $(u, v, w)$              | streamwise, vertical and spanwise velocity component                            |
| $\mathbf{u}$             | freestream velocity   |
| $(x, y, z)$              | streamwise, vertical and spanwise directions in the Cartesian coordinate system |
| $A_a$                    | acceleration due to added mass  |
| $A_b$                    | acceleration due to buoyancy  |
| $A_d$                    | acceleration due to drag  |
| $A_l$                    | acceleration due to lift  |
| $C_a$                    | coefficient of added mass   |
| $C_b$                    | coefficient of buoyancy   |
| $C_d$                    | coefficient of drag   |
| $C_l$                    | coefficient of lift   |
| $C_p$                    | pressure coefficient  |
| $\mathbf{N}(\mathbf{u})$ | nonlinear advection terms   |
| $Re$                     | Reynolds number   |
| $Re_b$                   | Reynolds number based on bubble relative velocity                               |
| $T$                      | total bubble tracking integration time  |

|                         |   |
|-------------------------|---|
| $U$                     | freestream velocity   |
| $\mathbf{U}_b$          | bubble velocity   |
| $\mathbf{U}_f$          | fluid velocity  |
| $\mathbf{U}_{rel}$      | relative velocity between bubble and fluid  |
| $\mathbf{X}_b$          | bubble position   |
| $\mathbf{X}_f$          | fluid element position  |
| $\alpha$                | angle of attack   |
| $\nu$                   | kinematic viscosity   |
| $\rho$                  | density   |
| $\boldsymbol{\omega}$   | vorticity   |
| $\boldsymbol{\omega}_z$ | vorticity in the spanwise direction   |
| $C$                     | arc of the simulation domain  |
| $\mathcal{N}$           | dimension between the simulation object and the out boundary of the simulation domain |

### INTRODUCTION

The production and entrainment of bubbles in ship wakes is not completely understood despite the fact that it affects the signature of the ship in military scenarios. Bubbles trapped in the large vortical structures in the ship wake can form clusters that are able to persist for large distances leaving a field signature. The bubbly wakes provide an excellent opportunity for wake homing torpedoes, to find their target because of the large acoustic cross section and high acoustic response of bubbles to acoustic waves. Bubbles can be produced by various mechanisms. According to Peltzer (1984) there are three major sources, including breaking or folding over of the bow wave, entrainment of air into the vessel's turbulent hull boundary layer at the surface and propeller rotation by drawing in air from the surface, racing in rough seaway or cavitation. Propeller plays a major part in the formation of bubbles and similar conclusions have also been made by Hsiao *et al.* (2006). With recent development of computer capability, understanding the behavior of bubbly flows by numerical simulation is becoming more common. The complicated behavior of bubbly propeller flow can be understood in a more fundamental manner by studying flow physics in hydrofoil wakes using direct numerical simulation (DNS). DNS can provide detailed information without the use of a turbulence model but at the expense of large amount of computation time and memory storage requirements. Thus, flows at Reynolds number ( $Re = Uc/\nu$ ) 200, 450 and 800 will be investigated. The Reynolds number is based on freestream velocity ( $U$ ) and hydrofoil chord length ( $c$ ), and hence time scales are made dimensionless by  $c/U$ .

In dispersed bubbly flow, two types of models are prevalent, the Eulerian-Lagrangian (particle tracking) and the Eulerian-Eulerian (two-fluid) models. In the Eulerian-Lagrangian model, liquid is treated as a continuous phase that is described in the Eulerian mode, and bubbles are treated as a dispersed phase that is tracked in the Lagrangian mode. In the Eulerian-Eulerian model, the dispersed bubbles are treated as a second continuous phase intermingled and interacting with the continuous liquid phase based on the concept of volume averaging with different velocities and volume fractions for each phase.

As has been noted by many researchers, flow structures can be significantly altered by the existence of bubbles due to the interaction between the bubble motion and the fluid dynamics (Serizawa *et al.*, 1975; Lance and Bataille, 1991). Johnson and Hsieh (1966) conducted a pioneering study of bubble trajectories in the early 1960s. Sridhar and Katz (1995) performed a more recent study to examine drag and lift forces on microscopic bubbles entrained by a vortex. The forces that act on bubbles as they are entrained by a vortex are measured using particle image velocimetry (PIV). The buoyancy, pressure and inertia forces were computed from the data, while the drag and lift forces are determined from a force balance on each bubble. Computed bubble trajectories compare well with experimental observations based on the measured lift and drag coefficients. Climent and Magnaudet (2006) investigated bubble dispersion in a two-dimensional upflowing mixing layer with Lagrangian tracking. The one-way coupling approach showed that characteristics of bubble dispersion are dominated by the capture of small bubbles within vortex cores due to the action of inertial forces. Two-way coupling simulations were carried out to study the effects by bubble induced disturbances on the motion of the flow field. Eulerian-Lagrangian models were used in the study of bubble columns (Vivek, Dhanannjay and Vivek, 2006; Hu and Celik, 2008) and the predicted data showed good agreement with classical experimental data. Smirnov *et al.* (2005) carried out simulation of bubble dynamics in wake flows with the Lagrangian particle dynamics (LPD) method. It was found that the method of LPD is most appropriate for computing bubble distributions in the ship wake due to relatively small volume fractions of bubble phase (Elghobashi, 1994; Crowe, 1998; Smirnov *et al.*, 2005). The results of the calculations showed that the bubbles tended to cluster in regions of high vorticity, which in turn could cause bubble coalescence and influence the flow itself. Hsiao *et al.* (2006) investigated effect of gas diffusion on bubble entrainment and dynamics around a propeller by the method of numerical simulation with Lagrangian particle tracking. Computations found that bubbles were seen to cluster in the vortices and blade wake regions, which is similar to the conclusions of Smirnov *et al.* (2005). It was also concluded that gas diffusion has important effect on bubble dynamics, especially the downstream bubble size distribution.

Besides the large body of work done on the Eulerian-Lagrangian models, Eulerian-Eulerian models have also been studied by other researchers. Cook and Harlow (1986) examined the properties of the von Karman vortex street for bubbly two-phase flow, assuming the density of gas in a bubble to be constant. Nishikawa *et al.* (1991) proposed a two-phase bubbly flow model. The two-phase

flow around an airfoil was calculated and it was reported that bubbles migrate from higher-pressure zone near the leading edge towards the lower-pressure zone near the trailing edge. Significant amount of work has been done on the Eulerian-Eulerian models with DNS for bubble-laden turbulent flows (Elghobashi, 1994; Druzhinin and Elghobashi, 1998; Druzhinin and Elghobashi, 1999). The motivation is that Eulerian-Lagrangian approach requires considerable computational resources when the instantaneous trajectories of a large number of individual bubbles need to be calculated, where using Eulerian-Eulerian reduces significantly the required computation expenses. Sugiyama *et al.* (2001) demonstrated the three-dimensional numerical analysis of two-phase bubbly flow over a circular cylinder under laminar flow conditions for Reynolds number from 100 to 2000. Bubbles accumulation in the Karman vortex and three-dimensional structures were observed. Uchiyama and Degawa (2007) conducted numerical simulation of air-water bubbly flow around a hydrofoil by vortex method with two-fluid flow approach. The computed results were in good agreement with the trend of experiment measurement. The same approach was applied to the air-water bubbly flow around two tandem square-section cylinder by Degawa and Uchiyama (2008). The strength of the Karman vortex was reduced due to the bubble entrainment. The simulation could predict the reduction of the drag force acting on the first cylinder that was clarified by the experimental study and results demonstrated that the vortex method with two-fluid approach is applicable to the bubbly flow analysis around a hydrofoil.

In summary, the Eulerian-Lagrangian models are sufficient if the bubble volume fraction is small, whereas Eulerian-Eulerian models are needed when the volume fraction is significant. Thus, the Eulerian-Lagrangian models are more suited for fundamental investigations of the bubbly flow (Pan *et al.*, 1999) while Eulerian-Eulerian models are usually preferred in industrial simulations (Portela and Oliemans, 2006). Despite considerable efforts for both models, accurate modelling of the two-phase flow remains an open question even for simple dispersed bubbly flow. The main objective of the study is to investigate the accuracy of current-state-of-art numerical models for simulating bubbly flows. The spectral element-Fourier code Semtex (Blackburn and Sherwin, 2004) will be used to solve the two-dimensional incompressible Navier-Stokes equations with Lagrangian particle tracking to investigate the effect of a hydrofoil on a population of bubbles as they pass over it, and the resulting distribution of bubbles downstream for a range of angles of attack and Reynolds numbers.

## MODEL DESCRIPTION

### Numerical Methods for Incompressible Flow

#### Governing Equations

The analytical techniques applied in this numerical study are associated with time-integration of the incompressible unsteady Navier-Stokes equations

$$\partial_t u = -N(u) - \frac{1}{\rho} \nabla p + \nu \nabla^2 u \quad (1)$$

$$\nabla \cdot u = 0 \quad (2)$$

where  $\mathbf{u} = \mathbf{u}(x, y, z, t) = (u, v, w)(t)$  is the velocity field,  $\mathbf{N}(\mathbf{u})$  represents nonlinear advection terms,  $p, \rho, \nu$  are respectively the fluid pressure, density and kinematic viscosity. The variable  $x, y, z$  and  $t$  are respectively the streamwise, vertical, spanwise and time coordinates and  $u, v, w$  are the velocity components in the streamwise, vertical and spanwise directions. The nonlinear terms are considered in skew-symmetric form  $\mathbf{N}(\mathbf{u}) = (\mathbf{u} \cdot \nabla \mathbf{u} + \nabla \cdot \mathbf{u} \mathbf{u})/2$ .

The velocity is assumed to be  $2\pi$ -periodic in the spanwise direction ( $z$ ), hence the velocity field can be projected exactly onto a set of two-dimensional complex Fourier modes

$$\hat{u}_k(x, y, t) = \frac{1}{2\pi} \int_0^{2\pi} u(x, y, z, t) \exp(-ik\theta) d\theta \quad (3)$$

where  $k$  is an integer wavenumber. The velocity field can be recovered from these complex modes through Fourier series reconstruction

$$u(x, y, z, t) = \sum_{k=-\infty}^{\infty} \hat{u}_k(x, y, t) \exp(ik\theta) \quad (4)$$

In practice, only a finite number of modes are retained in the calculation, and the conjugate-symmetric property of the Fourier transforms of real variables is exploited, so that the negative- $k$  modes are not required (Canuto *et al.*, 1988).

Equation (1) is subject to no-slip boundary conditions at the wall, a prescribed steady velocity at the inflow, conditions of zero pressure and zero outward normal derivatives of velocity at the outflow.

### Spatial Discretization and Time Integration

Spatial discretization is carried out in a Cartesian coordinate system (Figure 1), using standard nodal-Gauss-Lobatto-Legendre spectral element in the streamwise and vertical directions ( $x, y$ ), and Fourier expansions in the spanwise direction ( $z$ ) if required. This spatial discretization is coupled with a second-order-time velocity correction time-integration scheme.

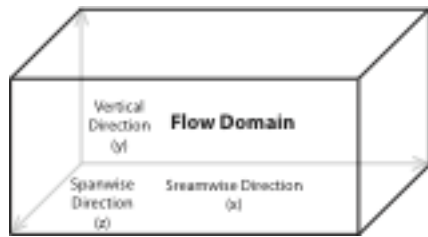


**Figure 1:** Simulation domain and coordinate system.

The spectral element methods can deal with arbitrary geometric complexity, and are capable of local mesh adaption by either increasing the number of elements or increasing the polynomial order with elements (Henderson, 1999). It takes advantage of the favourable convergence properties of interpolation using families of orthogonal polynomials and the Chebyshev and the Legendre polynomials are more commonly used among all. In the spectral element method, it uses the Gauss quadrature nodes and weights associated with the orthogonal polynomials that provide the linkage, and maintain the exponential convergence property

(Blackburn and Schmidt, 2003). Gauss-Lobatto quadrature nodes and weights are used in this case.

The use of Fourier expansion in the spanwise direction means that there is a one-to-one correspondence between wave number and Fourier mode index. Solutions can retain the option of projecting back to full set of Fourier modes if required. One single cell is used in the spanwise direction, as only the two-dimensional simulations will be conducted for the current study.

The time integration used is a projection scheme that is based on backwards differencing in time. As originally described (Karniadakis *et al.*, 1991), this was characterized as an operator-splitting scheme, but more recently it has been shown that the method is one of a class of velocity-correction projection scheme (Guermund and Shen, 2003). To keep the overall account here reasonably brief, the reader is referred elsewhere (Blackburn and Sherwin, 2004) for a detailed description of the method and resolution studies as applied to DNS.

### Simulation Conditions

The flow field around a NACA 0012 hydrofoil with chord length ( $c = 1$ ) at an angle of attack ( $\alpha$ ) is modelled in two dimensions. The circular inlet and outlet boundaries are located  $5c$  upstream and  $10c$  downstream. The width of the flow domain is  $10c$ .

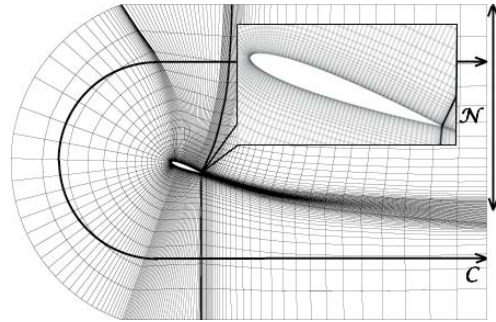


**Figure 2:** Simulation domain and the grid in proximity to the hydrofoil.

A C-type grid is used around the hydrofoil and summarized by the arc ( $C$ ), the dimension between the hydrofoil and the outer boundary ( $\mathcal{N}$ ). The cell counts are  $218 \times 35$  in these directions and a total of 7,630 elements in the two-dimensional domain are created. In each element, two-dimensional mapped tensor-product Lagrange-interpolant shape functions based on the Gauss-Lobatto-Legendre nodes are applied. At  $n_p = 5$  this elemental discretization corresponding to approximately 190,000 local degrees of freedom in the two-dimensional domain. The simulation domain and the grid in proximity to the hydrofoil are illustrated in Figure 2. A Dirichlet boundary condition of  $\mathbf{u} = (1, 0)$  is applied at the inlet, top and bottom boundaries. A Neumann boundary condition of  $\partial \mathbf{u} / \partial n = 0$  is applied at the outlet. The numerical artifacts such as domain and grid independence are ascertained for the present mesh by comparing the mean lift and drag coefficients with the literature values.

### Bubble Tracking Formulation

Considering relatively small amounts of bubble phase in the ship wakes, the method of Lagrangian particle tracking is most suitable for computing bubble distributions. It has advantages over the two-fluid model in the case of dilute suspensions or when large concentration variability of the discrete phase is present (Elghobashi, 1994; Crowe, 1998). This situation is true for bubbly wake flows, such as those in ship wakes, where bubbles may experience preferential concentration and clustering effects in the near wake region but are rather dilute in the far wake (Smirnov *et al.*, 2005).

### Massless Particle Tracking

The first step towards the complex bubble tracking is the massless particle tracking. Bubbles are treated as massless particle so that the bubble dynamics are simply defined by the flow dynamics

$$\frac{dX_b}{dt} = \frac{dX_f}{dt} = U_f \quad (5)$$

where  $X_b$  and  $X_f$  are the bubble position and fluid element position.  $U_f$  is the fluid velocity.

The predictor-corrector method will be used to solve Equation (5) to compute the position of massless bubbles. Numerical integration methods can be either explicit or implicit. Explicit methods are easy to use, but in general, the stability characteristics are not very good and as a result implicit methods may be preferred. However, for implicit methods, numerical solutions can only be calculated iteratively. The iteration will converge rapidly if a good initial guess can be provided. In order to reduce the iteration time and maintain stability, the explicit Adams-Bashforth predictor is used to predict a good initial guess, which can be used as the starting value for the iteration on the implicit Adams-Moulton corrector.

### Lagrangian Particle Tracking

In a more general model, bubbles in the flow field experience the combined effects of the carrying fluid flow and the buoyancy force. Thus, bubble trajectories are different from fluid element paths and precise force balance acting on the bubbles is required. Bubble trajectories are obtained using the bubble motion equation from Sridhar and Katz (1995) as shown in Equation (6). This is because the parameters of a single bubble dynamics in simple vortices were directly measured and these data represent the features of pure bubble dynamics.

$$\frac{dU_b}{dt} = A_a + A_b + A_d + A_l \quad (6)$$

where  $A_a$ ,  $A_b$ ,  $A_d$  and  $A_l$  are the accelerations due to added mass, buoyancy, drag and lift respectively, and they are given by the following expressions

*Added mass:* The acceleration due to added mass is

$$A_a = C_a \left( \frac{\partial U_f}{\partial t} + (U_f \cdot \nabla) U_f \right) \quad (7)$$

The coefficient of added mass ( $C_a$ ) is found to be 3.0, provided the bubble is nearly spherical (Sridhar and Katz, 1995).

*Buoyancy:* The acceleration due to buoyancy is

$$A_b = -C_b g \quad (8)$$

The coefficient of added mass ( $C_b$ ) is found to be 2.0 (Sridhar and Katz, 1995).

*Drag:* The acceleration due to drag is

$$A_d = \frac{3}{4r_b} C_d |U_{rel}| U_{rel} \quad (9)$$

*Lift:* The acceleration due to lift is

$$A_l = \frac{3}{4r_b} C_l |U_{rel}|^2 \frac{U_{rel} \times \omega}{|U_{rel}| |\omega|} \quad (10)$$

Both the coefficients of drag ( $C_d$ ) and lift ( $C_l$ ) are empirical function of  $U_{rel}$  and bubble diameter ( $d_b$ ), which are obtained from experiments.

The drag coefficient ( $C_d$ ) can be taken from the empirical drag relationship (Almedeij, 2008)

$$C_d = \left[ \frac{1}{(\varphi_1 + \varphi_2)^{-1} + (\varphi_3)^{-1} + \varphi_4} \right]^{1/10} \quad (11)$$

where

$$\begin{aligned} \varphi_1 &= (24 \text{Re}_b^{-1})^{10} + (21 \text{Re}_b^{-0.67})^{10} + (4 \text{Re}_b^{-0.33})^{10} + (0.4)^{10} \\ \varphi_2 &= \frac{1}{(0.148 \text{Re}_b^{0.11})^{-10} + (0.5)^{-10}} \\ \varphi_3 &= (1.57 \times 10^8 \text{Re}_b^{-1.625})^{10} \\ \varphi_4 &= \frac{1}{(6 \times 10^{-17} \text{Re}_b^{2.63})^{-10} + (0.2)^{-10}} \end{aligned} \quad (12)$$

and  $\text{Re}_b$  is the Reynolds number based on bubble relative velocity ( $U_{rel}$ ) and bubble diameter ( $d_b$ ).

$$\text{Re}_b = \frac{U_{rel} d_b}{\nu} \quad (13)$$

The relationship is calibrated free of systematic error with experimental data available for  $\text{Re}_b < 10^6$ .

The coefficient of lifts ( $C_l$ ) was derived to be 0.53 (Auton, 1981). Sridhar and Katz (1995) calculated the magnitude of the lift coefficients that range from 0.1 to 0.3 and were found to be consistent with the study by Barkla and Auchterlonie (1971).

*Bassett force:* The Bassett force term involves a history integral and it is expected to be much smaller than the other dominant forces acting on bubbles (Ranade, 2002). Sridhar and Katz (1995) concluded that the contribution of the Bassett force is less than 6% of the buoyancy force. Consequently this force is neglected in this study.

## RESULTS

The results from massless particle tracking are presented in this paper, but the results from the model of Lagrangian particle tracking will be presented at the conference.

### Massless Particle Tracking

Nine bubble tracking cases at three different angles of attack ( $\alpha = 0^\circ, 10^\circ$  and  $20^\circ$ ) and three different Reynolds numbers ( $Re = 200, 450$  and  $800$ ) have been studied. Simulations start in the two-dimensional flow domain and bubbles are not initiated until the flow field reaches steady state or periodic shedding. A time step of  $h = 0.0005$  is

used and a total of 150 bubbles are continuously released on each side of the hydrofoil surface with an interval of 200 time steps.

**Angle of attack at  $\alpha = 0^\circ$**

Figure 3 present the bubble tracking results at  $\alpha = 0^\circ$  with  $Re = 200, 450$  and  $800$ . The bubbles released from the upper surface of the hydrofoil are marked in red and those from the lower surface are in blue. For all three cases, bubbles flow along the hydrofoil surface, as the fluid flow is parallel to the surface. They flow almost straight into the wake of the hydrofoil. As the Reynolds number increases, the vortices on both side of the hydrofoil are stretched further downstream but no vortex shedding is observed at this angle of attack.

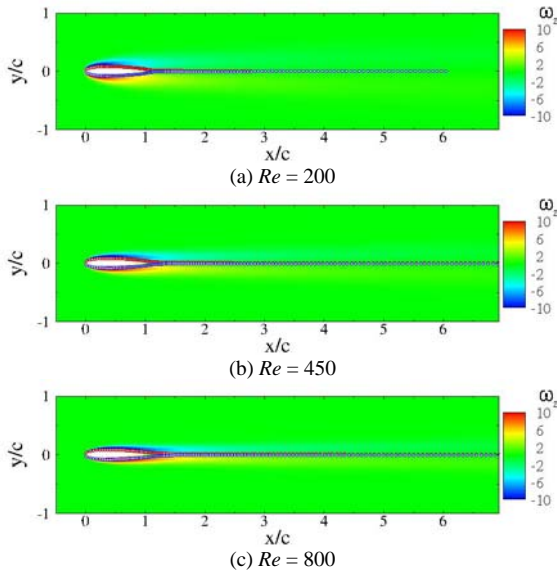


**Figure 3:** Effect of Reynolds number on downstream bubble distribution with vorticity contour at  $\alpha = 0^\circ$ .

**Angle of attack at  $\alpha = 10^\circ$**

Bubble tracking results at  $\alpha = 10^\circ$  are presented in Figure 4. Flow separates from the upper surface of the rear half at  $Re = 200$ . As the Reynolds number increases, the separation point moves towards the leading edge. At  $Re = 200$  and  $450$ , bubbles flow straight into the wake of the hydrofoil. At  $Re = 800$ , flow becomes unsteady and vortices developed from upper and lower surfaces shed alternatively and convect downstream. Bubbles are meandering in the wake behind the trailing edge of the hydrofoil.

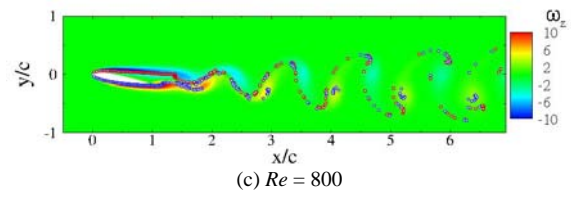
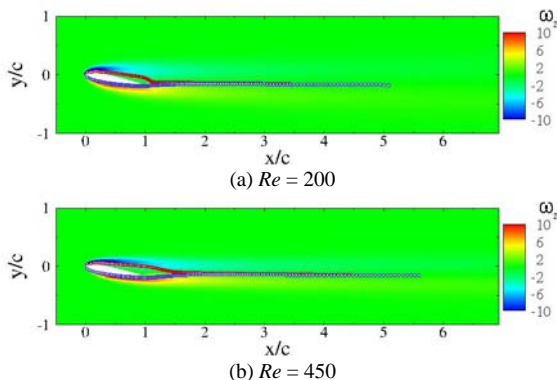


**Figure 4:** Effect of Reynolds number on downstream bubble distribution with vorticity contour at  $\alpha = 10^\circ$ .

**Angle of attack at  $\alpha = 20^\circ$**

Bubble tracking results at  $\alpha = 20^\circ$  are presented in Figure 5. The flow separation from the upper surface is confirmed in all three cases. For  $Re = 200$ , the bubbles released near the leading edge from the upper surface are entrained into the reverse flow region above the trailing edge of the hydrofoil. They clustered with the bubbles released from the lower surface at the trailing edge propagate downstream together with the vortices developed from the trailing edge of the hydrofoil. For  $Re = 450$  and  $800$ , strong vortex shedding from both upper and lower surfaces are observed. The bubbles released from the upper surface are entrained in the vortices developed from the leading edge of the upper surface and the bubbles released from the lower surface are entrained in the vortices developed from the trailing edge of the hydrofoil. Bubbles are meandering in the wake and forming clusters in the vortices behind the hydrofoil.

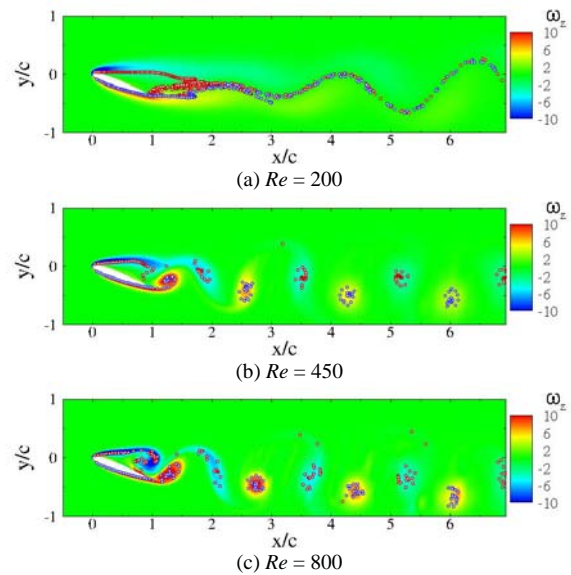


**Figure 5:** Effect of Reynolds number on downstream bubble distribution with vorticity contour at  $\alpha = 20^\circ$ .

**CONCLUSION**

The bubbly flow around a NACA0012 hydrofoil is simulated with the massless particle tracking algorithm at three different angles of attack ( $\alpha = 0^\circ, 10^\circ$  and  $20^\circ$ ) and three different Reynolds numbers ( $Re = 200, 450$  and  $800$ ). When the angle of attack  $\alpha$  is  $0^\circ$ , the flow is parallel to the hydrofoil surface and there is no vortex shedding behind the hydrofoil. Bubbles flow along the hydrofoil surface. When the angle of attack  $\alpha$  is  $10^\circ$ , the flow separates from the upper-surface and the separation point moves towards the leading edge of the hydrofoil as the

Reynolds number increases. At  $Re = 800$ , vortex shedding is observed and bubbles meander in the wake. When the angle of attack  $\alpha$  is  $20^\circ$ , the flow separates near the leading edge of the upper surface and large eddies are shed from both the upper and lower surfaces. The bubbles are entrained to form clusters in the vortices behind the hydrofoil.

A more detailed and realistic Lagrangian particle tracking algorithm based on the bubble motion equation from Sridhar and Katz (1995) will be implemented and further studies will be conducted using this model. With the success of the massless particle tracking, the Lagrangian particle tracking will be carried out to perform the fundamental study of the bubbly flow over a hydrofoil. It provides a better model to study the effects of the hydrofoil, for a range of angles of attack and Reynolds numbers, on the downstream bubble distribution.

## REFERENCES

- Almedeij, J., (2008), "Drag coefficient of flow around a sphere: Matching asymptotically the wide trend", *Powder Technology*, **186**, 218–223.
- AUTON, T. R., (1981), "The dynamics of bubbles, drops and particles in motion in liquids", *Ph.D. Thesis*, Cambridge University, Cambridge, UK.
- BARKLA, H. M. and AUCHTERLONIE, L. J., (1971), "The Magnus or Robins effect on rotating sphere", *J. Fluid Mech.*, **47**, 437.
- BLACKBURN, H. M. and SCHMIDT, S., (2003), "Spectral element filtering techniques for large eddy simulation with dynamic estimation", *J. Comput. Phys.*, **186**, 610–629.
- BLACKBURN, H. M. and SHERWIN, S. J., (2004), "Formulation of a Galerkin spectral element-Fourier method for three-dimensional incompressible flows in cylindrical geometries", *J. Comput. Phys.*, **197**, 759–778.
- CANUTO, C., HUSSAINI, M. Y., QUARTERONI, A. and ZANG, T. A., (1988), "Spectral methods in fluid dynamics", Springer Berlin 2nd edition.
- CLIMENT, E., and MAGNAUDET, J., (2006), "Dynamics of a two-dimensional upflowing mixing layer seeded with bubbles: Bubble dispersion and effect of two-way coupling", *Phys. Fluids*, **18(10)**, 103304.
- COOK, T. L. and HARLOW, F. H., (1986), "Vortices in bubbly two-phase flow", *Int. J. Multiphase Flow*, **12**, 35–61.
- CROWE, C. T., (1998), "An assessment of multiphase flow models for industrial applications", *volume FEDSM-5093*, Washington, DC, USA. In: Proceeding of FEDSM.
- DEGAWA, T. and UCHIYAMA, T., (2008), "Numerical simulation of bubbly flow around two tandem square-section cylinders by vortex method", *Proc. Inst. Mech. Eng. Part C J. Mech. Eng. Sci.*, **222**, 225–234.
- DRUZHININ, O. A. and ELGHOBASHI, S., (1998), "Direct numerical simulations of bubble-laden turbulent flow using the two-fluid formulation", *Phys. Fluids*, **10(3)**, 685–697.
- DRUZHININ, O. A. and ELGHOBASHI, S., (1999), "A Lagrangian-Eulerian mapping solver for direct numerical simulation of bubble-laden turbulent shear flows using the two-fluid formulation", *J. Comput. Phys.*, **154**, 174–196.
- ELGHOBASHI, S., (1994), "On predicting particle-laden turbulent flows", *Appl. Sci. Res.*, **52**, 309–329.
- GUERMOND, J. and SHEN, J., (2003), "Velocity-correction projection methods for incompressible flows", *SIAM Journal on Numerical Analysis*, **41(1)**, 112–134.
- HENDERSON, R. D., (1999), "Adaptive spectral element methods for turbulence and transition", in: Barth, T. J. and DECONINCK, H. (Eds), "High-order methods for computational physics", Springer, Berlin, 225–324.
- HSIAO, C. T., JAIN, A. and CHAHINE, G. L., (2006), "Effect of gas diffusion on bubble entrainment and dynamics around a propeller", *In 26th Symposium on Naval Hydrodynamics*, Rome, Italy.
- HU, G. and CELIK, I., (2008), "Eulerian-Lagrangian based large-eddy simulation of a partially aerated flat bubble column", *Chem. Eng. Sci.*, **63**, 253–271.
- JOHNSON, V. E. and HSIEH, T., (1966), "The influence of the trajectories of gas nuclei on cavitation inception", *In 6th Symposium on Naval Hydrodynamics*, 163–179.
- KARNIADAKIS, G. E., ISRAELI, M. and ORSZAG, S. A., (1991), "High-order splitting methods for incompressible Navier-Stokes equations", *J. Comput. Phys.*, **97(2)**, 414–443.
- LANCE, M. and BATAILLE, J., (1991), "Turbulence in the liquid phase of a uniform bubbly air-water flow", *J. Fluid Mech.*, **222**, 95–118.
- NISHIKAWA, H., MATSUMOTO, Y. and OHASHI, H., (1991), "Numerical calculation of the bubbly two-phase flow around an airfoil", *Comput. Fluids*, **19**, 453–460.
- PAN, Y., DUDUKOVIC, M. P. and CHANG, M., (1999), "Dynamic simulation of bubbly flow in bubble columns", *Chem. Eng. Sci.*, **54(13)**, 2481–2489.
- PELTZER, R. D., (1984), "White-water wake characteristics of surface vessels", *Naval Research Laboratory Memorandum Report*, 5335.
- PORTELA, L. M. and OLIEMANS, R. V. A., (2006), "Possibilities and limitations of computer simulations of industrial turbulent dispersed multiphase flows", *Flow Turbul. Combust.*, **77**, 381–403.
- RANADE, V. V., (2002), "Computational flow modelling for chemical reactor engineering", *Academic Press*, London.
- SERIZAWA, A., KATAOKA, I. and MISHIGOSHI, I., (1975), "Turbulence structure of air-water bubbly flow-I. Measuring techniques", *Int. J. Multiphase Flow*, **2**, 221–233.
- SMIRNOV, A., CELIK, I. and SHI, S., (2005), "LES of bubble dynamics in wake flows", *Comput. Fluids*, **34**, 351–373.
- SRIDHAR, G. and KATZ, J., (1995), "Drag and lift forces on microscopic bubbles entrained by a vortex", *Phys. Fluids*, **7(2)**, 389–399.
- SUGIYAMA, K., TAKAGI, S. and MATSUMOTO, Y., (2001), "Three-dimensional numerical analysis of bubbly flow around a circular cylinder", *JSME Int J., Ser. B*, **44(3)**, 319–327.
- UCHIYAMA, T. and DEGAWA, T., (2007), "Vortex simulation of the bubbly flow around a hydrofoil", *International Journal of Rotating Machinery*, 2007, 1–9.
- VIVIEK, V., DHANANNJAY, S. D. and VIVIEK, V. R., (2006), "Eulerian-Lagrangian simulations of unsteady gas-liquid flows in bubble columns", *Int. J. Multiphase Flow*, **32**, 864–885.